Proceedings of ICRC 2001: 1301 © Copernicus Gesellschaft 2001

ICRC 2001

Radiofrequency properties of antarctic ice and calibration of the RICE detector

D. Seckel[1], **G. Spiczak**[1], **S. Seunarine**[2], **G. M. Frichter** [3], **C. Allen**[4], **D. Besson**[4], **D. J. Box** [4], **R. Buniy**[4], **E. Copple**[4], **D. McKay** [4], **J. Ralston** [4], **D. W. Schmitz** [4], **and I. Kravchenko**[5]

[1]Bartol Research Institute, U. of Delaware, Newark DE 19716
[2]Department of Physics and Astronomy, Private Bag 4800, U. of Canterbury, Christchurch, New Zealand
[3]Florida State University, High Energy Physics, Tallahassee FL 32306-4350
[4]University of Kansas Dept. of Physics and Astronomy, Lawrence KS 66045-2151
[5] Massachusetts Institute of Technology Lab. for Nuclear Science, Cambridge, MA 02139

Abstract. The RICE experiment (Radio Ice Cherenkov Experiment) at the South Pole, co-located with the AMANDA experiment, seeks to detect ultra-high energy (UHE) electron neutrinos producing radio-frequency Cherenkov radiation in cold polar ice. We describe calibration procedures used to measure the neutrino flux.

1 Introduction

The RICE experiment presently consists of an 18-channel array of radio receivers ("Rx"), scattered within a 200 m×200 m×200 m cube, at 100-300 m depths. Nine receivers are buried in the boreholes drilled for the AMANDA photomultiplier tube deployment during the 1996-97, 97-98, and 99-00 austral summers. Six receivers are located in dedicated RICE holes; four such holes were drilled with a mechanical hole-borer in 1998-99. The signal from each antenna is boosted by a 36-dB in-ice amplifier, then carried by ∼300 m coaxial cable to the surface observatory, where the signal is filtered (suppressing noise below 200 MHz), re-amplified (either 52- or 60-dB gain), and fed into a CAMAC crate. After initial discrimination (using a LeCroy 3412E discriminator), the signal is routed into a NIM crate where the trigger logic resides. A valid trigger signal initiates readout of receiver waveforms, as recorded on HP54542 digital oscilloscopes. Also deployed are three large TEM surface horn antennas which are used as a veto of surface-generated noise.

2 Timing Calibration and $\epsilon(\omega)$ Measurement

Event and source reconstruction is based on our knowledge of the array geometry, ice properties and thus the expected times a wave-front propagates from the source to any given receiver location. Knowing the time differences δt_{ij} between all pairs (i, j) of hit antennas we perform χ^2 minimization to find the source location and source direction. For the full reconstruction this method requires at least four antennas to be hit (i.e., $3\delta t_{ij}$ values). Uncertainties in δt_{ij} arise from several sources, including risetime resolutions (∼10-20 ns), differences in signal propagation velocity in the ice due to variations in the dielectric constant with depth, differences in signal propagation speed within the different analog cables being used, differences in cable lengths, and deployment surveying uncertainties.

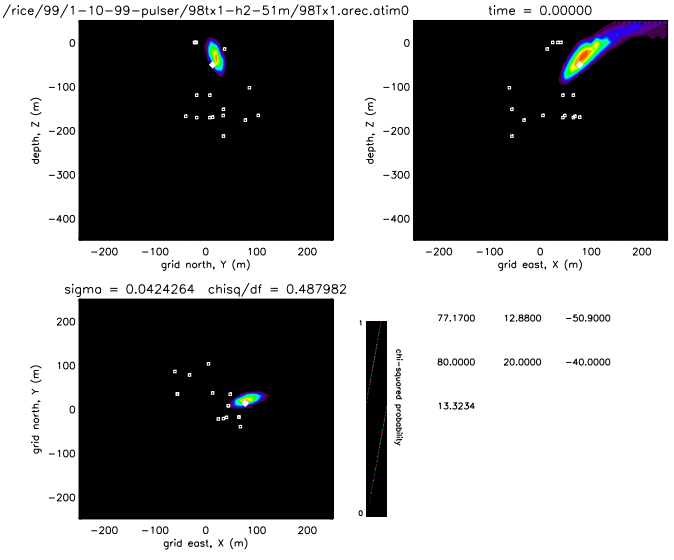

Fig. 1. Reconstruction of Tx pulse, based exclusively on measured receiver times. Diamond indicates surveyed location of transmitter; color intensity code indicates χ^2 of reconstruction. Open white squares indicate receivers.

Buried transmitters ("Tx") are used to calibrate the channel-to-channel timing delays. A 5 ns duration pulse is sent to one of the five transmitters, which subsequently broadcasts the signal to the receiver array. An event vertex is reconstructed exclusively from the measured time delays; comparison with the actual transmitter location allows a calculation of the tim-

Correspondence to: Dave Besson (dbesson@ku.edu)

ing residual χ^2 for each channel, based on the timing uncertainty $\sigma_t(ij)$: $(\frac{\delta t_{ij}^{\rm measured} - \delta t_{ij}^{\rm expected}}{\sigma_t(ij)})^2$. An iterative procedure is used to calibrate out the observed channel-to-channel timing delays and minimize the timing residuals for an ensemble of events. Typical timing calibration corrections are ∼20 ns per channel. A calibration event is shown in Figure 1. Here the χ^2 probability is calculated over a 3 dimensional grid (grid bin size = 10m) of possible vertex points; the grid corresponds to a cube 500 meters on a side. Three orthogonal 2 dimensional slices, each passing though the minimum value of χ^2 are shown. The colors indicate likelihoods ranging from near zero (black) to near unity (red). Small squares indicate the positions of RICE receivers and the white diamond indicates the surveyed position of the RICE transmitter 96Tx1 which emitted the reconstructed pulse. In this case the difference between surveyed and reconstructed event vertex is about 13m. The spatial residual, at this very early level of calibration, is typically 10 meters, which is consistent with the intrinsic resolution of our calibration technique.

2.1 Measurement of Refractive Index

The complex dielectric constant $\epsilon(\omega)$ allows one to calculate both the absorptive and refractive effects of the ice. The imaginary part of the dielectric constant (the "loss tangent") prescribes losses due to absorption; the real part corresponds to the refractive index of the medium. Information on the refractive index can be derived from temperature and density profiles acquired by AMANDA deep drilling operations. Such profiles ($z(T,\rho)$) can be combined with laboratory measurements of the dependence of the index of refraction of ice on temperature and density ($n(T,\rho)$) to predict the expected index of refraction profile at the South Pole as a function of depth $n(z)$. This derived $n(z)$ function can be compared with the profile calculated directly from RICE transmitter data. Using the surveyed transmitter and receiver locations, combined with Fermat's principle, one can determine the profile $n(z)$ which reproduces the observed $Tx \rightarrow Rx$ radio signal transit times. The comparison between the measured $n(z)$ function determined from transmitter data with the "derived" $n(z)$ profile is shown in Figure 2. Agreement is satisfactory.

Absorption of radio waves in cold glacial ice is temperature, density, and frequency dependent and has been measured (Bogorodsky and Gavrilo, 1980), indicating attenuation lengths α ∼1-10 km. at frequencies in the range 100 MHz – 1 GHz. Given the small scale of our current array (∼100 m) compared to the very large attenuation length α expected for Polar ice in the 100 MHz – 1 GHz regime, our baseline is insufficient to reproduce previous measurements of α in cold polar ice; long baseline transmitter measurements are an objective of future campaigns.

3 Antenna Response and Gain Calibration

Although the neutrino search analysis is, at this point, based only on channel-to-channel timing (Seckel, 2001), the amplitude calibration is needed in order to ensure that the discriminator efficiency, as a function of threshold voltage setting, is reliably calculable. I.e., for a neutrino of a given energy at a given distance from an antenna, we need to be certain that the array is sensitive to the resulting Cherenkov signal.

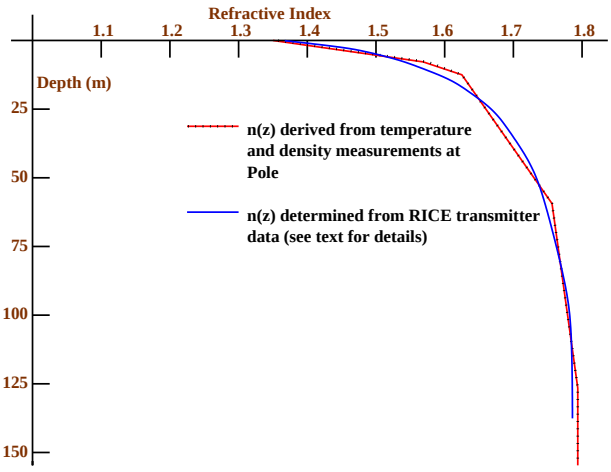

Fig. 2. Index of refraction as a function of depth.

One of the fundamental parameters used to define any antenna is the effective area $A_{eff}(\theta,\phi)$; this is related to the incident Cherenkov signal intensity I as: $P_{out} = IA_{eff}$. The full antenna performance is usually characterized as either an effective area $A_{eff}(\theta,\phi)$ or a complex effective height $\boldsymbol{h}(\theta,\phi)$. The effective area and the magnitude of the complex effective height can be related through: $|\boldsymbol{h}| = \sqrt{ZA_{eff}/(120\pi)}$ $(= \sqrt{Z\lambda^2(Gain)/(480\pi^2)})$, where the impedance Z has been normalized to 50Ω. The polarization of $\boldsymbol{h}$ is aligned along the dipole axis $\hat{n}_A$ as $\boldsymbol{h} = h\hat{n}_A$, where h is the magnitude of effective height. The complex effective height $\boldsymbol{h}$ (in units of meters) is simply related to both the magnitude and the phase of the voltage resulting from the application of a complex electric field vector at the antenna load by: $V_{out} = \boldsymbol{E}_{in}\cdot\boldsymbol{h} = h\boldsymbol{E}_{in}\cdot\hat{n}_A$. The full, complex transfer function $\boldsymbol{T}(\omega)$ for the antenna, in principle, gives a complete description of the antenna (+cable) response. This function $\boldsymbol{T}(\omega)$ can be written as the product of the complex impedance of the (antenna+cable) $\boldsymbol{Z}(\omega)$ multiplied by the complex height function $\boldsymbol{h}(\omega)$, properly taking into account potential mismatches between the impedance of the antenna and the impedance of the attached cable: $\boldsymbol{T} = \boldsymbol{h}(Z_{cable})/(\boldsymbol{Z}_{antenna} + Z_{cable})$, with Z_{cable}=50Ω+i0Ω. Both the magnitude and phase of the effective height are both determined directly from measurements made on the KU Antenna Testing Range (KUATR); $\boldsymbol{Z}_{antenna}$ is determined from reflected power measurements on a Network Analyzer (NWA).

On the Testing Range, a transmitter broadcasts a signal of known strength and phase to a receiver; the receiver response is recorded by a NWA. The magnitude of the effective height measured for a typical RICE dipole is given in Figure 3. The peak frequency (∼600 MHz) is roughly consistent with the dimensions of the half-dipole (∼15 cm); the effective height,

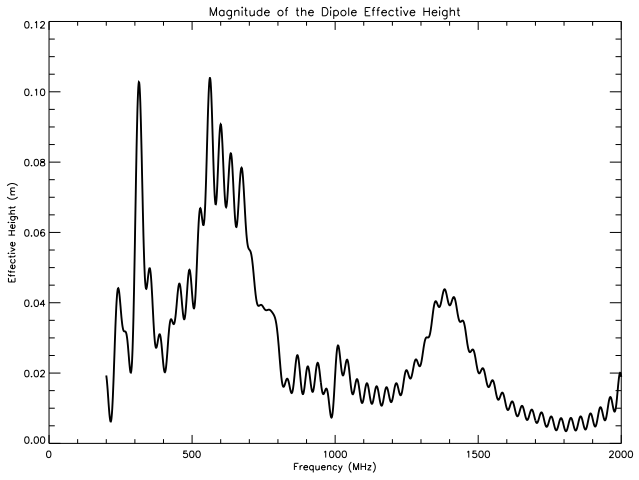

Fig. 3. Modulus of RICE dipole effective height (m.) as a function of frequency.

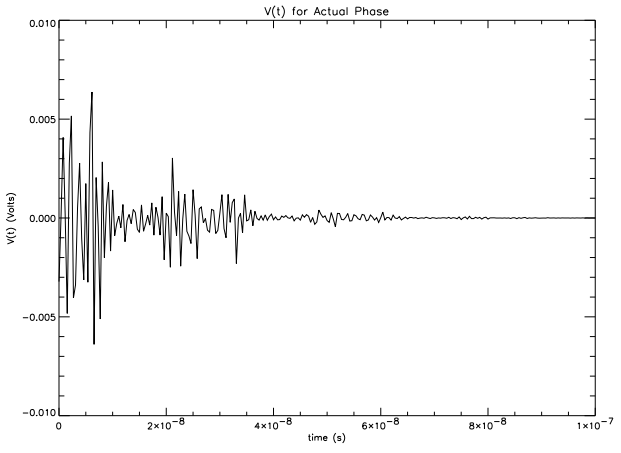

Fig. 4. Expectation for observed RICE signal shape V'(t) based on measured effective height and complex impedance function, given a delta function input signal to a RICE antenna.

as expected, also has magnitude of order 10 cm. at the peak frequency.

The phase variation of the effective height has also been measured as a function of frequency at KUATR; approximately: $\Delta\phi(\phi) \approx 0.031\phi$ (rad). (Note that, neglecting this phase variation with frequency can only result in an overestimate of the antenna sensitivity to a broadband, narrow-duration time pulse, since the calculated antenna sensitivity would therefore neglect destructive interference between different frequency components.) Given the magnitude of the effective height, the phase variation of the effective height, and the magnitude and phase variation of the complex antenna impedance $\boldsymbol{Z}(\omega)$, the complex transfer function $\boldsymbol{T}(\omega)$ can now be calculated, and used to predict the expected waveform observed in a RICE antenna in response to a narrow impulsive signal. This is done by transforming the input impulse $V(t)$ to frequency space, multiplying the function $V(\omega)$ by the transfer function $\boldsymbol{T}(\omega)$ (properly normalized), and then transforming back to the time domain to give $V'(t)$. Figure 4 shows the result of this exercise. Qualitatively, the after-pulsing observed in data (Seckel, 2001) is reproduced by our complex transfer function, although we stress that the actual expected signal shape observed requires knowledge of the details of the input signal.

Dipole response has also been measured as a function of both azimuthal and polar angles. The polar angle response is observed to be well approximated by a $cos^2\theta$ dependence (in power); the dipole response in azimuth is observed to be flat, as expected.

3.1 Amplifier Gain Calibration

Signals from the antennas are boosted by two stages of amplification, totalling from between +88 dB – +96 dB of gain, depending on the channel. For a RICE waveform containing only ("unbiased") thermal noise, the total power in a frequency interval ΔB can be calculated from the discrete Fourier transform of the waveform as $P_{noise} = kT\Delta B$ (we check several 50 MHz-wide frequency bins from 250 to 500 MHz for this calculation). Since the total noise power in this band at the input to the antenna can also be written as $P_{<V>} = \Sigma\frac{V^2}{Z}$, we can relate $P_{<V>} = P_{noise}G$, where G is the overall gain of the system. Thus, based on the rms voltage $< V >$ of the 8192 samples contained in these "unbiased" waveforms, the gain of the amplifiers can be calculated *in situ*. The amplifier gain measured this way is flat up to the bandwidth limit of the oscilloscopes (500 MHz); direct laboratory measurements of the amplifier gain using a network analyzer are consistent with flat response up to 750 MHz. Most(>90%) of the amplifiers are stable to 1-2 dB over the course of data-taking thus far analyzed.

3.2 Full Circuit Amplitude Calibration

In the final step of our amplitude calibration, the antenna response to a continuous wave (CW) signal broadcast from an under-ice transmitter is measured *in situ*. This test calibrates the combined effects of all cables, signal splitters, amplifiers, etc. in the array. A 1 milliwatt (0 dBm) continuous wave signal is broadcast through the transmit port of an HP8713C NWA. The NWA scans through the frequency range 0→1000 MHz in 200 bins, producing a 0 dBm CW signal in each frequency bin. The signal is transmitted through ∼1000 feet of coaxial cable to one of the five under-ice dipole transmitting antennas. The transmitters subsequently broadcast this signal to the under-ice receiver array, and the return signal power from each of the receivers (after amplification, passing through cable and fed back into the return port of the NWA) is then measured. Using laboratory measurements made at KUATR of: a) the effective height of the dipole antennas, as a function of frequency (previously described), b) the dipole Tx/Rx efficiency as a function of polar angle and azimuth, c) cable losses and dispersive effects (cables are observed to be non-dispersive for the lengths of cable,

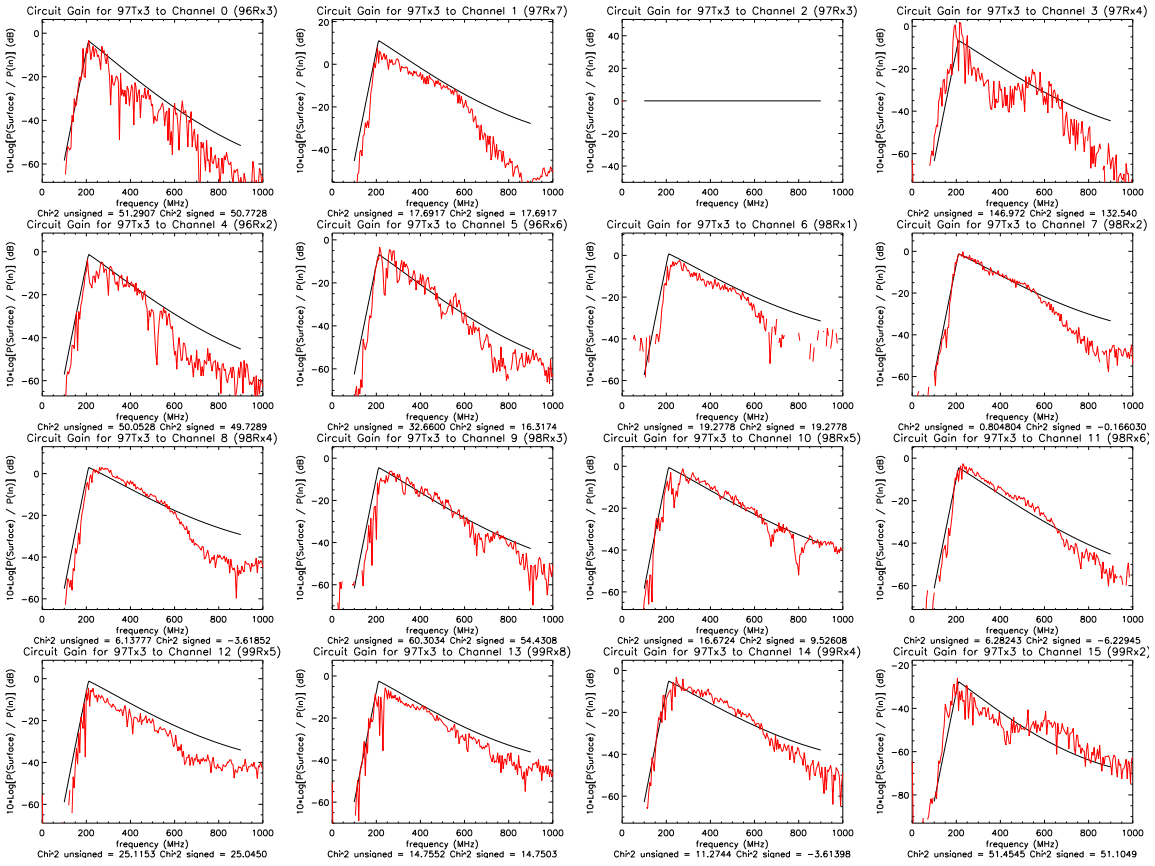

Fig. 5. Comparison of expected (solid curve) vs. measured (histogram) Tx→Rx signal strength for one transmitter broadcasting to 16 receivers. Vertical scale is Return-Power/Transmit-Power, in dB. No data is shown for the receiver (channel 3, top row) in the same hole as the transmitter being used for this test, due to possible cross-talk effects. Corrections for the measured roll-off of surface amp gain for some channels above 700 MHz have also not been made.

and over the frequency range used in this experiment), d) the gain of the two stages of amplification as determined from RICE data acquired *in situ* by normalizing to thermal noise $P_{noise} = kT\Delta B = \Sigma < V_{ant}^2 > /Z$), and e) finally correcting for $1/r^2$ spherical spreading of the signal, one can model the receiver array and calculate the expected signal strength returning to the input port of the network analyzer. This can then be directly compared with actual measurement. Such a comparison, as a function of frequency, is shown in Figure 5 for one transmitter (97Tx3). Below 200 MHz, the attenuating effect of the high-pass filter is evident. Within the "analysis" frequency band of our experiment (200 MHz - 500 MHz), our level of uncertainty in the total circuit power is ± 6 dB. Note that, for the case of a neutrino event, this uncertainty can be considered to be conservative, as it folds in effects of both the receiver and the transmitter.

In sum, a first-pass calibration of both the time and amplitude response of RICE radio receivers has been made, relying primarily on data taken *in situ*. The calibration of the detector is sufficient to allow limits to be placed on the incident high-energy neutrino flux.

Acknowledgements. We gratefully acknowledge the logisitical support of the AMANDA Collaboration, the National Science Foundation Office of Polar Programs, the University of Kansas, the University of Canterbury Marsden Grant, and the Cottrell Research Corporation. Matt Peters of the U. of Texas SOAR group provided invaluable consultation on antenna design, calibration and electrical engineering. We also thank the winterovers who staffed the experiment during the last two years at the South Pole (Xinhua Bai, Darryn Schneider and Steffen Richter). Ryan Dyer helped in deployment during the 1999-2000 campaign. We are indebted to Dan DePardo and Dilip Tammana for their help in setting up and operating the KU Antenna Testing Range.

References

V . V. Bogorodsky and V. P. Gavrilo, *Ice: Physical Properties*, Modern Methods of Glaciology (Lenningrad, 1980); V. V. Bogorodsky, C. R. Bentley and P. E. Gundmandsen, "Radioglaciology", Reidel Publishing (1985).

D. Seckel, *et al.*, these proceedings (2001).